Supplement of Earth Surf. Dynam., 9, 1–18, 2021
https://doi.org/10.5194/esurf-9-1-2021-supplement

Earth Surface Dynamics
Open Access
EGU

Supplement of

Groundwater erosion of coastal gullies along the Canterbury coast (New Zealand): a rapid and episodic process controlled by rainfall intensity and substrate variability

Aaron Micallef et al.

Correspondence to: Aaron Micallef (amicallef@geomar.de)

Optically Stimulated Luminescence (OSL) methodology

Sample preparation and analytical facilities

Luminescence samples were prepared under subdued red light condition in the luminescence laboratory from Cluj-Napoca, Romania. The material from the ends of each sample tube was used for gamma spectrometry and water content measurements whereas polymineral fine grains (4-11 µm) and coarse (63-90 µm) K-feldspars were extracted from the inner part. Samples were first treated with hydrochloric acid (10% concentration) for calcium carbonate removal, followed by a treatment with hydrogen peroxide (30% concentration) in order to remove the organic matter. All samples were wet sieved in order to collect the finer (<63 µm) and coarser (>63 µm) grains. Polymineral fine grains (4-11 µm) were obtained by settling using Stoke's law and centrifuging in distilled water (Frechen et al., 1996; Lang et al., 1996). Coarser grains in the range of 63-90 µm was obtained through dry sieving. For coarse K-rich feldspars extraction, an etching with HF (10% concentration) for 40 min was employed to remove the coating and alpha irradiated layer, and the material was then rinsed for 40 min with HCl (10% concentration) to remove any precipitated fluorides. K-feldspar enriched extracts were then separated using a heavy liquid solution with $\rho<2.58$ g/cm^3.

Luminescence analyses were performed using TL/OSL Risø DA-20 reader equipped with automated detection and stimulation head (DASH) (Lapp et al., 2015). Luminescence signals were detected by PDM 9107Q-AP-TTL-03 (160-630 nm) photomultiplier. A blue filter combination (Schott BG36+Corning 7-59, with transmission between 320-460 nm) was used for the detection of polymineral fine grains and K-feldspar signals. Laboratory irradiations were carried out using a calibrated ^{90}Sr/^{90}Y beta source delivering 0.0764 Gy/s for fine grains and 0.086 Gy/s for coarse grains. K-feldspar coarse grains were mounted on stainless steel discs using silicone oil as an adhesive while for polymineral fine grains aluminium discs were used.

Equivalent dose determination

Equivalent doses on polymineral fine grains and K-feldspar coarse grains were determined using post-IR IRSL protocols based on SAR procedure with two different preheat and post-IR IRSL stimulation temperature combination ($pIRIR_{290}$ and $pIRIR_{225}$). For equivalent dose determination using $pIRIR_{290}$ protocol (see Table S1a) (Buylaert et al., 2011a; Buylaert et al., 2012; Buylaert et al., 2011b; Thiel et al., 2011) samples were preheated for 60 s at 320 °C and stimulated with IR diodes for 200 s at 50 °C to reduce the signal that is prone to fading by allowing recombination of near-neighbour trap and centre pairs. A subsequent IR stimulation at 290 °C for 200 s was employed in order to record the signal of interest. A high-temperature bleach was performed for 100 s at 325 °C at the end of each cycle.

Table S1: Flowchart of the $pIRIR_{290}$ (Buylaert et al., 2011a; Buylaert et al., 2012; Buylaert et al., 2011b; Thiel et al., 2011) and $pIRIR_{225}$ (Buylaert et al., 2009; Vasiliniuc et al., 2012) protocols applied in this study.

step	a. $pIRIR_{290}$	b. $pIRIR_{225}$
1	Dose	Dose
2	Preheat (320˚C; 60s)	Preheat (250˚C; 60s)
3	IRSL (50˚C; 200s)	IRSL (50˚C; 200s)
4	IRSL (290˚C; 200s)	IRSL (225˚C; 200s)
5	Test dose	Test dose
6	Preheat (320˚C; 60s)	Preheat (250˚C; 60s)
7	IRSL (50˚C; 200s)	IRSL (50˚C; 200s)
8	IRSL (290˚C; 200s)	IRSL (225˚C; 200s)
9	IRSL (325˚C; 100s)	IRSL (290˚C; 100s)

The second protocol used for equivalent dose determination was $pIRIR_{225}$ protocol (see Table S1b) (Buylaert et al., 2009; Vasiliniuc et al., 2012), which involves a preheat of 250 °C for 60s and an IR stimulation, firstly at 50 °C for 200s and then at 225 °C for 200s. The test dose response was determined in the same way. In order to reduce the residual charge, a bleaching at 290 °C for 100s was performed at the end of each cycle.

The size of the test dose used for equivalent dose determination varied between 20% and 50% of the equivalent dose value.

Annual dose determination

The radionuclide activity concentration was determined using high-resolution gamma spectrometry with a well-HPGe detector. The samples were stored for one month in order to achieve equilibrium between ^{226}Ra and ^{222}Rn. The conversion factors tabulated by Guérin et al. (2011) were used in determining the annual dose rates. For polymineral fine grains, an alpha efficiency factor of 0.08±0.02 was assumed. The water content was assumed to be 15% with a relative error of 25%. The total dose rates include the external contribution from beta and gamma radiation (additionally alpha radiation for 4-11 μm), as well as from the cosmic rays. The dose rates of cosmic rays were determined as a function of depth, altitude and geomagnetic latitude (Prescott and Hutton, 1994). An internal beta dose was included in the dose rate for K-feldspars, calculated assuming a K-content of 12.5±0.5%. For polymineral fine grains (4-11 μm) it was assumed that any dose rate derived from internal alpha activity is negligibly small. The radionuclide activity concentration and the annual doses for both samples are presented in Table S2.

Table S2: Summary of the $pIRIR_{225}$ and $pIRIR_{290}$ ages obtained on polymineral fine grains (4-11 µm) and coarse K-feldspars (63-90 µm) and dosimetry data. The ages were determined considering 15% water content.

	ED-pIRIR225		ED-pIRIR290		Gamma Spectrometry			Annual dose		Age (ka)-pIRIR225		Age (ka)-pIRIR290	
Sample code	pfg	K-feld. (63-90 µm)	pfg	K-feld. (63-90 µm)	Th-232	Ra-226	K-40	pfg	K-feld. (63-90 µm)	pfg	K-feld. (63-90 µm)	pfg	K-feld. (63-90 µm)
NZ 13A	55.5 ±1.9	60.6 ±1.6	72.7 ±3.3	78.8 ±3.3	29.3 ±0.9	32.9 ±0.7	530 ±17	3.48± 0.06	3.01± 0.04	**16.0±1.4**	**20.1±1.5**	**20.9±2**	**26.2±2.1**
NZ 14A	16.1 ±0.5	5.6± 0.2	20.9 ±1.7	9.5± 0.7	29.3 ±1.1	31.5 ±1.0	518 ±14	3.48± 0.06	3.03± 0.04	**4.6±0.4**	**1.9±0.1**	**6.0±0.7**	**3.1±0.3**

Fading test

It is well known that the infrared stimulated luminescence (IRSL) signal from feldspars is prone to fading (Wintle, 1973). Anomalous fading is a decrease of the IRSL signal with time, being a result of quantum mechanical tunnelling (Visocekas, 1985). Thus, the IRSL ages tend to underestimate the depositional age. In order to check if the IRSL signals from NZ13A and NZ14A samples were stable in time, 3 aliquots for each sample were used for the fading rates (percentage of the signal lost per decade of time (Aitken, 1985)) measurements using $pIRIR_{225}$ protocol. The aliquots used for g-value measurements were first utilized in residual dose determination. Each aliquot was irradiated with a beta dose of 50 Gy. A test dose of 25 Gy was used throughout all fading measurements. Prior to fading measurements, four consecutive prompt readouts were carried out. The IRSL signals of interest were then read-out after a preheat treatment and different storage times. After the longest storage time of 48 hours, two consecutive readouts were carried out.

Luminescence properties

Representative laboratory growth curves constructed for polymineral fine (Fig. S1a, c) grains as well as for coarse K-feldspars (Fig. S1b,d) from sample NZ13A using $pIRIR_{225}$ and $pIRIR_{290}$ protocols are shown in Fig. S1. The dose response curves were well fitted using a sum of two saturating exponential functions. For all aliquots measured, the recycling ratios were within 10% from unit indicating that the test dose signal successfully corrects for sensitivity changes during the repeated SAR cycles. As can be seen in the insets of Fig. S1, the decay of the natural and a regenerative signal have similar patterns. The recuperation ratios are small (<5%) for all aliquot measured.

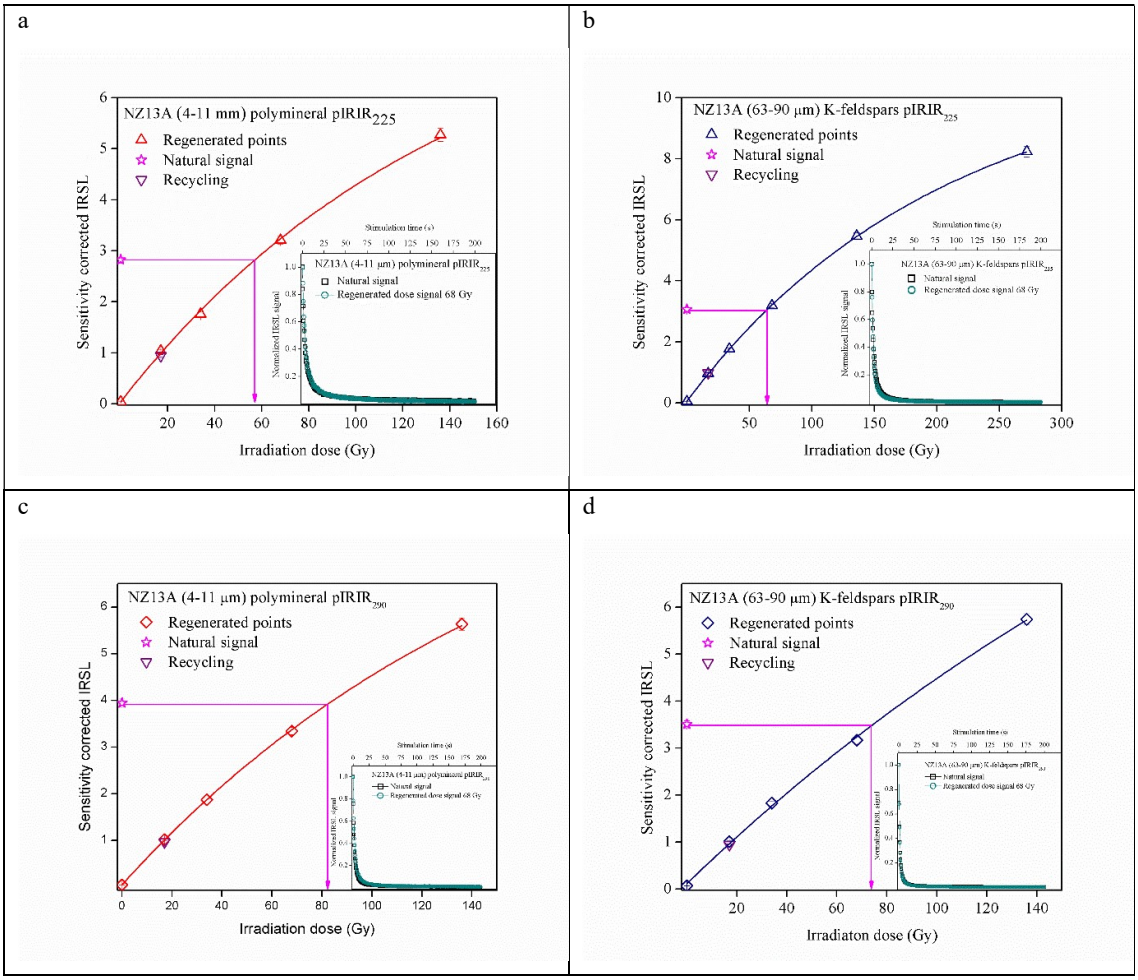

Figure S1: Representative sensitivity-corrected dose response curves constructed for sample NZ13A using one aliquot of (a) polymineral fine grains, (b) coarse K-feldspars using pIRIR$_{225}$ protocol and (c) polymineral fine grains, (d) coarse K-feldspars using pIRIR$_{290}$ protocol. The sensitivity corrected natural signal is represented as a star and the arrow indicates the equivalent dose. Recycling points are presented as an inverse triangle. The inset show a typical decay curve of natural IRSL signal (open square) in comparison to a regenerated signal (open circles) induced by a beta dose approximately equal with the equivalent dose.

Residual doses

Previous studies in literature have reported difficulties in bleaching the natural pIRIR signals even after prolonged exposure in daylight or in a solar simulator, obtaining residual doses of a few Gy (Buylaert et al., 2011b; Lowick et al., 2012; Roberts, 2012).

In order to determine the residual doses, three to five fresh aliquots were exposed for 20 days to daylight. The residual doses obtained for polymineral fine grains are 3.3±0.3 Gy (NZ13A) and 3.0±0.2 Gy (NZ14A) using pIRIR$_{225}$ protocol and 10±1 Gy (NZ13A) and 11±1 Gy (NZ14A) using pIRIR$_{290}$ protocol. In the case of coarse K-feldspars residual doses of 2.9±0.1 Gy (NZ13A) and 1.3±0.1 Gy (NZ14A) was obtained using pIRIR$_{225}$ protocol

and 9.0±0.3 Gy (NZ13A) and 4.9±0.3 Gy (NZ14A) using $pIRIR_{290}$ protocol. Similar values for the residual doses have been reported so far in literature. Murray et al. (2014) reported $pIRIR_{290}$ residual doses ranging between 4.5±0.3 and 10.1±0.1 Gy for loess samples collected from Serbia, SE Europe and Sohbati et al. (2016) measured an average residual dose of 6.15±0.10 Gy using $pIRIR_{290}$ protocol on loess samples from New Zealand, South Island. Also, low residual doses were obtained using $pIRIR_{225}$ protocol by Buylaert et al. (2009) for samples with various sedimentary origins.

Dose recovery

The most stringent test for any SAR protocol is the dose recovery test (Murray, 1996; Murray and Wintle, 2003; Wallinga et al., 2000), that analyses whether the protocol can successfully measure a known irradiation dose prior to any thermal treatment.

A dose recovery test was performed on five aliquots for polymineral fine grains and five aliquots on coarse K-feldspars for each sample (NZ13A and NZ14A) using both protocols ($pIRIR_{225}$ and $pIRIR_{290}$). The fresh aliquots were exposed for 21 days to daylight in order to remove the natural signals. Laboratory known doses were chosen to be approximately equal to the measured equivalent dose. The dose recovery ratios were calculated after the residual doses were subtracted from the measured dose. The size of the test dose used for dose recovery measurements varied between 20-50% of the size of the given dose. Figure S2 shows the results for the dose recovery test for sample NZ13A (Fig. S2a) and NZ14A (Fig. S2b). The ratios between the recovered and given dose for polymineral fine grains are 1.11±0.03 (NZ13A) and 1.01±0.03 (NZ14A) using $piRIR_{225}$ protocol and 1.14±0.05 (NZ13A) and 1.03±0.06 (NZ14A) using $pIRIR_{290}$ protocol. In the case of coarse K-feldspars, the dose recovery ratios are 0.96±0.01 (NZ13A) and 0.87±0.03 (NZ14A) using $pIRIR_{225}$ protocol, while those obtained by applying $pIRIR_{290}$ protocol are 1.17±0.06 (NZ13A) and 1.16±0.04 (NZ14A). We conclude that the overall behaviour of the $pIRIR_{225}$ protocol is satisfactory whereas the $pIRIR_{290}$ protocol overestimates the given dose by ~ 17%.

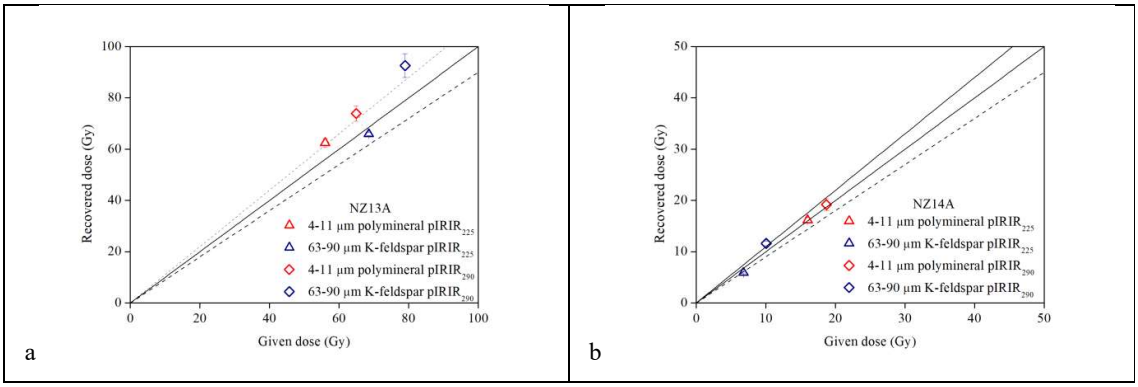

Figure S2: Dose recovery test results for polymineral fine grains and coarse K-feldspars using $pIRIR_{225}$ and $pIRIR_{290}$ protocols for (a) NZ13A and (b) NZ14A samples. The given doses were chosen to be approximately equal to the equivalent dose for each sample. The solid line indicates the ideal 1:1 dose recovery ratio while the dash lines represent a 10% variation from unity.

Equivalent doses

The equivalent doses measured on polymineral fine grains as well as on coarse K-feldspars grains using $pIRIR_{225}$ and $pIRIR_{290}$ protocols are displayed in Table 2. For NZ13A sample an equivalent dose of 55.5±1.9 Gy and 60.6±6 Gy was measured using $pIRIR_{225}$ protocol on polymineral fine grains and coarse K-feldspars, respectively.
For the same sample, the equivalent dose using $pIRIR_{290}$ protocol is 72.7±3.3 Gy on polymineral fine grains while on coarse K-feldspars a value of 78.8±3.3 Gy was obtained. In the case of NZ14A sample, the equivalent doses obtained using $pIRIR_{225}$ protocol are 16.1±0.5 Gy on polymineral fine grains and 5.6±0.2 Gy on coarse K-feldspars, whereas using $pIRIR_{290}$ protocol are 20.9±1.7 Gy on polymineral fine grains and 9.5±0.7 Gy on coarse K-feldspar. The equivalent doses presented in Table 2.

g-values

g-values were measured for both samples (NZ13A and NZ14A) using $pIRIR_{225}$ protocol. Negative g-values were obtained for polymineral fine grains in the case of these two samples. For coarse K-feldspars an average g-value for sample NZ13A was 0.60±0.5%/decade, while for sample NZ14A the measured value was that of 0.85±0.09%/decade. Figure S3 shows the results obtained for the fading measurement for a representative aliquot from sample NZ13A for polymineral fine grains (Fig. S3a) and coarse K-feldspars (Fig. S3b). As it can be seen in Fig. S3, the measured sensitivity corrected IRSL signals after different delay time's scatter in the range of the signals obtained after the 6 prompt readouts. We conclude that such low fading rates represent laboratory artefact and do not accurately reflect the signal stability in nature (Buylaert et al., 2012; Roberts, 2012; Thiel et al., 2011). Therefore the ages presented in this study were the ones not corrected for fading.

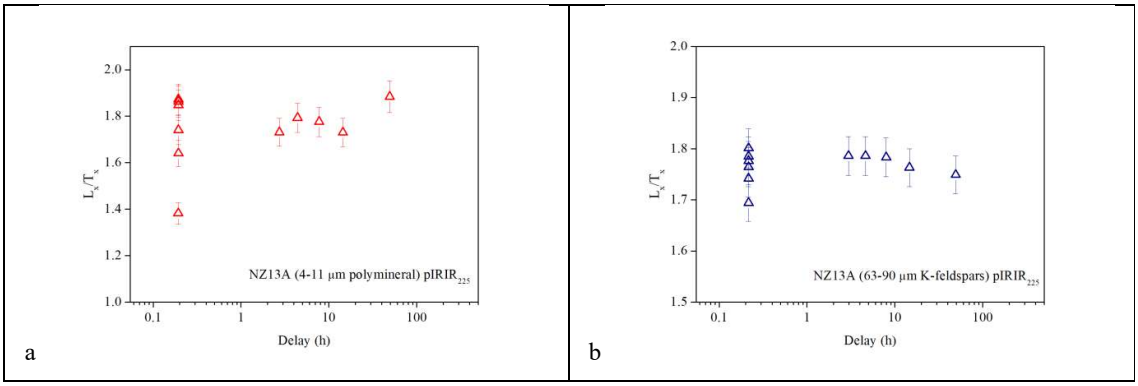

Figure S3: Results of the fading rates measurement using $pIRIR_{225}$ protocol on one representative aliquot from sample NZ13A for (a) polymineral fine grains and (b) coarse K-feldspars. A maximum delay of 48 hours was used for both samples. A number of 4 consecutive prompt readouts were carried out before signal measurement after delay and two consecutive prompt readouts were added after the 48 hours delay.

Various values of the fading rates were reported in literature for the IRSL signal measured using $pIRIR_{225}$. g-values >1 %/decade were obtained (Buylaert et al., 2009; Thomsen et al., 2008; Zhang et al., 2018), while Vasiliniuc et al. (2012) calculated g-values ranging from 0.6 to 1.3 %/decade. Previous studies reported low fading

rates (<1%/decade) measured by using $pIRIR_{290}$ protocol. Sohbati et al. (2016) measured g-values of 0.9±0.3 %/decade for New Zealand loess, while Thiel et al. (2011) reported g-values considered to be laboratory artefact for Austrian loess.

2-D G-TEM slingram modelling

An extensive attempt was made to fit a 1-D electrical conductivity model to the G-TEM slingram responses acquired with the 10 × 10 m TX loop and TX-RX offset 30 m at the study area. However, this attempt proved unsuccessful and it was concluded that the underlying geoelectrical structure cannot be a simple plane-layered medium. A 1-D model does not generate the changes in sign of the ramp-off voltage response of the type shown in Figure S4. The solid symbols in the plots correspond to a positive voltage recorded at the RX coil, whereas open symbols correspond to a negative voltage.

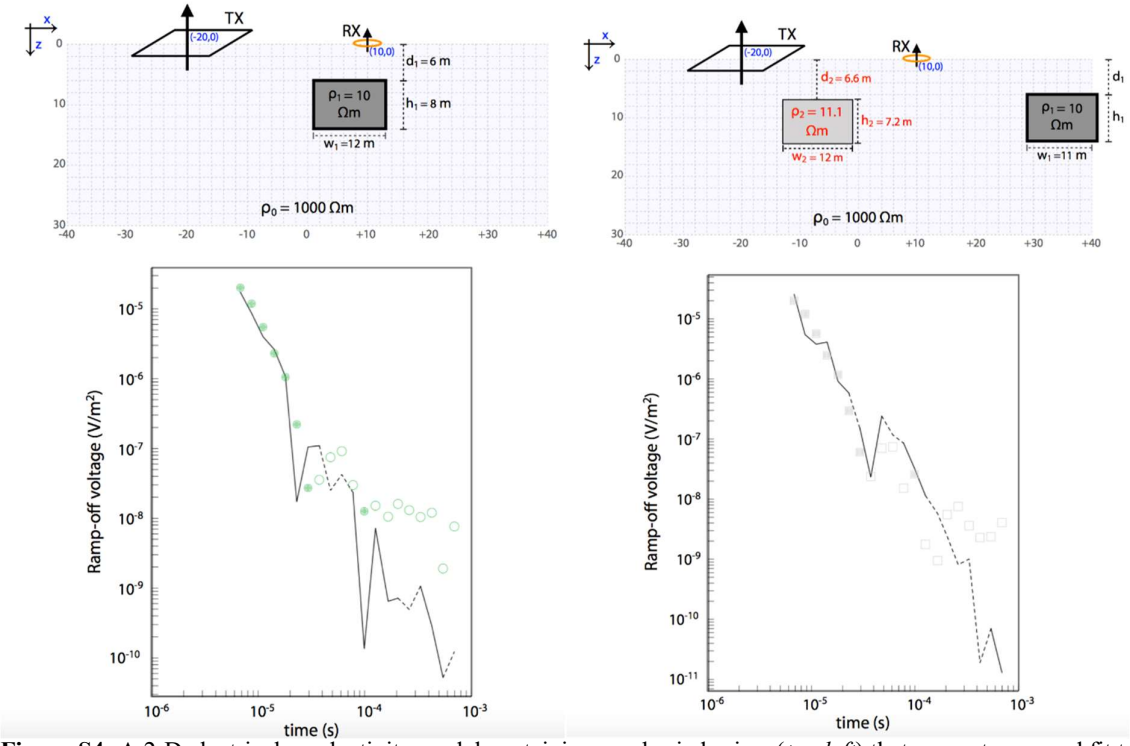

Figure S4: A 2-D electrical conductivity model containing one buried prism (*top left*) that generates a good fit to G-TEM slingram response at station 160 on transect May 15-1; (*bottom left*); a 2-D model with two prisms (*top right*) fitting the response at station 130 (*bottom right*). The units of the top figures are in metres. In the bottom figures, the solid portion corresponds to a positive response and the dashed portion corresponds to a negative response.

Shown at the top left of Figure S4 is a 2-D electrical conductivity model containing a buried conductive prism of resistivity 10 Ωm, height 8 m, width 12 m and, with its top buried at a depth of 6 m below the surface. The resistivity of the host material is 1000 Ωm. The TX-RX offset is 30 m. The centre of the prism is located at 36 m from the centre of the TX loop. The strike length of the buried prism, in and out of the plane of the paper, is infinite.

A 3-D finite-element (FE) modelling program (Pondthai et al. 2020) was used to simulate the G-TEM slingram response of a number of models containing an infinitely long buried prism like the one shown. The prism models

we explored were motivated by the inversion results of the nearby 40 × 40 m TX loop soundings, made with the RX coil placed at the centre of the loop, which consistently show a conductive zone at ~10 m depth enclosed by a resistive host.

Shown at the bottom left of the figure, for the prism shown at the top left, is the FE-computed response in the solid and dashed lines. The green symbols indicate the measured G-TEM slingram response from the station located at 160 m from the start of transect May 15-1. Note that the simulated response of this prism provides a good match to the measured response, especially reproducing the transition from a positive to negative response at time-gate 7 (~3×10^{-5} s after TX ramp off). The conductive prism is interpreted as a buried groundwater conduit, as discussed in the main text of the paper.

It was found that the single-prism model was able to provide a good fit to the G-TEM responses for much of the May 15-1 transect from the station at 140 m all the way to the end of the line. However, the fit of this model degrades at stations that are closer to the start of the line. At stations at a distance of 120-140 m, for example, after much trial and error, it was found that a two-prism model is more capable of producing a good match to the data. For example, the measured G-TEM response at station 130 m is shown at the bottom right of the figure. At this station, the single prism of the initial model is located well to the right of the RX coil. This prism was augmented by a second prism, with slightly different model parameters to those of the first, located in-between the TX loop and RX coil as shown in the top right of the figure. The FE-computed G-TEM response of the 2-prism model is shown by the solid/dashed lines in the bottom right. A good fit is found to the observations, again especially at the change in sign of the ramp-off voltage at time gate 7. Note that the FE-computed response of a model containing only the second prism at the left does not produce such a good fit; in fact, both prisms are needed to fit the data.

These 2-D modelling examples are included in these supplementary materials principally to demonstrate that 2-D geoelectrical structures can explain the complex, sign-changing G-TEM slingram responses measured along the Ashburton coast. More extensive 2-D modelling is beyond the scope of this paper but will be elaborated in a future publication. The resulting 2-D geoelectrical structures will provide a sharper perspective on the hidden geometry of the subsurface groundwater conduits feeding the box canyons.

References:

Aitken, M. J.: Thermoluminescence dating, Academic Press, Orlando, 1985.

Buylaert, J.-P., Murray, A. S., and Thomsen, K. J.: Testing the potential of an elevated temperature IRSL signal from K-feldspar, Radio Measurements, 44, 560-565, 2009.

Buylaert, J.-P., Huot, S., Murray, A. S., and Van Den Haute, P.: Infrared stimulated luminescence dating of an Eemian (MIS 5e) site in Denmark using K-feldspar, Boreas, 40, 46-56, 2011a.

Buylaert, J.-P., Jain, M., Murray, A. S., Thomsen, K., Thiel, C., and Sohbati, R.: A robust feldspar luminescence dating method for Middle and Late Pleistocene sediments, Boreas, 41, 2012.

Buylaert, J. P., Thiel, C., Murray, A. S., D., V., Yi, S., and Lu, H.: IRSL and post-IR IRSL residual doses recorded in modern dust samples from the Chinese Loess Plateau, Geochronometria, 38, 432-440, 2011b.

Frechen, M., Schweitzer, U., and Zander, A.: Improvements in sample preparation for the fine grain technique, Ancient TL, 14, 15-17, 1996.

Guérin, G., Mercier, N., and Adamiec, G.: Dose-rate conversion factors: Update, Ancient TL, 29, 5-8, 2011.

Lang, A., Lindauer, S., Kuhn, R., and Wagner, G. A.: Procedures used for optically and infrared stimulated luminescence dating of sediments in Heidelberg, Ancient TL, 14, 7-11, 1996.

Lapp, T., Kook, M., Murray, A. S., Thomsen, K., Buylaert, J. P., and Jain, M.: A new Luminescence Detection and Stimulation Head for the Risø TL/OSL reader, Radiation Measurements, 81, 178-184, 2015.

Lowick, S. E., Trauerstein, M., and Preusser, F.: Testing the application of post IR-IRSL dating to fine grain waterlain sediments, Quaternary Geochronology, 8, 33-40, 2012.

Murray, A. S.: Developments in optically stimulated luminescence and photo-transferred thermoluminescence dating of young sediments: application to a 2000-year sequence of flood deposits, Geochimica et Cosmochimica Acta, 60, 565-576, 1996.

Murray, A. S., and Wintle, A. G.: The single aliquot regenerative dose protocol: potential for improvements in reliability, Radiation Measurements, 37, 377-381, 2003.

Murray, A. S., Schmidt, E. D., Stevens, T., Buylaert, J. P., Marković, S. B., Tsukamoto, S., and Frechen, M.: Dating Middle Pleistocene loess from Stari Slankamen (Vojvodina, Serbia) – Limitations imposed by the saturation behaviour of an elevated temperature IRSL signal, Catena, 117, 34-42, 2014.

Pondthai, P., Everett, M.E., Micallef, A., Weymer, B.A., Faghih, Z., Haroon, A., Jegen, M.:3D characterization of a coastal freshwater aquifer in SE Malta (Mediterranean Sea) by time-domain electromagnetics, Water, 12(6), 1566, 2020.

Prescott, J. R., and Hutton, J. T.: Cosmic ray contribution to dose rates for luminescence and ESR dating: large depths and long term variations, Radiation Measurements, 23, 497-500, 1994.

Roberts, H. M.: Testing Post-IR IRSL protocols for minimising fading in feldspars, using Alaskan loess with independent chronological control, Radiation Measurements, 47, 716-724, 2012.

Sohbati, R., Borella, J., Murray, A., Quigley, M., and Buylaert, J.-P.: Optical dating of loessic hillslope sediments constrains timing of prehistoric rockfalls, Christchurch, New Zealand, Journal of Quaternary Science, 31, 678-690, 2016.

Thiel, C., Buylaert, J.-P., Murray, A., Terhorst, B., Hofer, I., Tsukamoto, S., and Frechen, M.: Luminescence dating of the Stratzig loess profile (Austria) – Testing the potential of an elevated temperature post-IR IRSL protocol, Quaternary International, 234, 23-31, 2011.

Thomsen, K. J., Murray, A. S., Jain, M., and Bøtter-Jensen, L.: Laboratory fading rates of various luminescence signals from feldspar-rich sediment extracts, Radiation Measurements, 43, 1474-1486, 2008.

Vasiliniuc, Ș., Vandenberghe, D. A. G., Timar-Gabor, A., Panaiotu, C., and Cosma, C.: Testing the potential of elevated temperature post-IR IRSL signals for dating Romanian loess, Quaternary Geochronology, 10, 75-80, 2012.

Visocekas, R.: Tunneling radiative recombination in laboradorite. Its association with anomalous fading of thermoluminescence, Nuclear Tracks and Radiation Measurement, 10, 521-529, 1985.

Wallinga, J., Murray, A. S., and Wintle, A. G.: The single-aliquot regenerative-deose (SAR) protocol applied to coarse-grain feldspar, Radiation Measurements, 32, 529-533, 2000.

Wintle, A. G.: Anomalous fading of thermoluminescence in minerals, Nature, 245, 143-144, 1973.

Zhang, J., Rolf, C., Wacha, L., Tsukamoto, S., Durn, G., and Frechen, M.: Luminescence dating and palaeomagnetic age constraint of a last-glacial loess-paleosol sequence from Istria, Croatia, Quaternary International, 494, 19-33, 2018.